Efficient Full-Wave Analysis of Stratified Planar Structures and Unbiased TW-FET's

Marco Farina, Giampiero Gerini, *Member, IEEE,* and Tullio Rozzi, *Fellow, IEEE*

Abstract—**We have developed a rigorous full-wave analysis technique capable of characterizing quasiplanar travelling wave structures, constituted of multilayer dielectrics and conductors of finite thickness, also taking into account dielectric and conductor losses. We have studied boxed embedded microstrips and another complex passive structure, namely the T-gate TW-FET, devoting particular attention to the distribution of current inside the metallization. All structures considered were simulated by means of a desktop computer. We have tested our program by comparing our results with experimental data of embedded microstrips and employed it for the characterization of planar and T-type gates of the FET's without bias.**

I. Introduction

THE development of monolithic integrated circuits for millimeter waves (MMIC's) requires analysis methods of increasing accuracy and efficiency. In as much as these features set opposite requirements, an adequate compromise is usually possible only for relatively simple structures; this is particularly true for the case of active devices such as the TW-FET, that is a distributed wideband amplifier, making use of waves growing along the length of the device. A major factor in the characterization of this structure are the losses introduced by the gate electrodes [1]. In fact the gate cross-section is rather small, causing such high loss as to render practically impossible to achieve distributed gain by means of the standard gate MESFET [2].

On the other hand, straightforward widening of the gate is accompanied by a rapid deterioration of the transconductance, that is inversely proportional to the electrode width.

Employing a T-gate partly remedies the above drawbacks by reducing the metal contact with the epitaxial layer on the one hand, while increasing the conductor section on the other.

As recently shown in [3], [4], the usual perturbation techniques fail in the analysis of structures of this kind; this happens because the concept of "skin effect" loses its meaning in situations where both dimensions of the conductor cross-section are not negligible. Moreover, high losses in the MMIC structures also have a strong influence on the dispersion characteristics.

Various rigorous analysis techniques were employed to study planar structures, such as the FDTD method [5]; the computational effort involved is, however, considerable, particularly when dealing with MMIC's, because of the fine meshes required.

Manuscript received December 27, 1993; revised December 2, 1994.

The authors are with the Dipartimento di Elettronica ed Automatica, Università degli Studi di, Ancona, 60131 Ancona, Italy.

IEEE Log Number 9410714.

Quasi-TEM approaches are analytical and offer a certain degree of accuracy: models including the active operation of TW-FET's where also developed, as in [6] and [7]; unfortunately, the nearly total exclusion of multilayer situations imposes intolerable constraints on the range of validity of such approximations.

One of the few alternative approaches to the heavy numerical methods currently in use was proposed by Heinrich in [3]: it is self consistent and is based on mode matching. Still, even this approach is practically restricted in application by the computational complexity of mode matching.

The approach here presented allows a rigorous evaluation of losses and dispersion characteristics through the solution of an integral eigenvalue equation.

The latter is obtained by imposing that fields within the box loaded by lossy dielectrics also satisfy the boundary conditions imposed by the presence of lossy metallizations. The eigenfunctions of said eigenvalue equation give the current distributions within the conductors.

This method is as rigorous as that of [3], but with a considerable degree of added flexibility in as much as the computational load does not increase proportionally to the number and complexity of the dielectric and conducting layers.

Comparison of results with existing numerical and experimental data for the microstrip line shows excellent agreement. We have also investigated by this approach unbiased TW-FET structures, with standard gate and T-gate, as proposed in the literature, taking in account the effect of the depletion region under the gate and of the highly doped regions required for ohmic contacts.

II. Analysis

A. Eigenvalue Equation

Let us consider a configuration of N conductors arbitrarily located within a multilayer dielectric slab. The dielectrics are characterized by a complex permittivity

$$\varepsilon_i = \varepsilon_{ri}\varepsilon_0 - j\frac{\sigma_i}{\omega}.$$

The conductor cross-sections are of fairly arbitrary shape in principle, even though in the following we shall consider combinations of rectangles; the structure is enclosed in a metal box.

The first step consists in replacing the conductors with distributed currents. We then construct the dyadic Green's function (DGF) suitable for distributed current sources, linking the latter to the electric field. Considering the dielectric

stratification to be in the y-direction, it is expedient to express the DGF by means of vector potentials oriented along y. This amounts to assuming y as direction of transverse propagation and reduces the DGF to a form expressible in terms of two scalar potentials, which, in turn, can be expanded in terms of the eigenfunctions of a parallel plate waveguide along the y-direction [8].

Consequently, we write

$$\mathbf{E}(\mathbf{r}) = -\tilde{\mathbf{Z}} \cdot \mathbf{J}(\mathbf{r}) \tag{1}$$

where $\tilde{\mathbf{Z}}$ is a dyadic integral operator whose kernel is given by

$$\begin{aligned} &-j\omega\varepsilon(y)\mathbf{Z}(\mathbf{r},\mathbf{r}') \\ &= \left(\hat{\mathbf{y}}\hat{\mathbf{y}} + \frac{\nabla_t\nabla_t}{\nabla_t^2}\right)\delta(\mathbf{r}-\mathbf{r}') \\ &\quad + (\nabla\times\nabla\times\hat{\mathbf{y}})(\nabla'\times\nabla'\times\hat{\mathbf{y}})S_{\mathrm{LSM}}(\mathbf{r},\mathbf{r}') \\ &\quad + k^2(\nabla\times\hat{\mathbf{y}})(\nabla'\times\hat{\mathbf{y}})S_{\mathrm{LSE}}(\mathbf{r},\mathbf{r}') \end{aligned} \tag{2a}$$

and

$$j\omega\varepsilon(y')S_{\mathrm{LSM}}(\mathbf{r},\mathbf{r}') = \sum_i \frac{\Phi_i(x,z)\Phi_i^*(x',z')}{k_{ti}^2} Y_{\mathrm{LSM}_i}(y,y') \tag{2b}$$

$$j\omega\mu S_{\mathrm{LSM}}(\mathbf{r},\mathbf{r}') = \sum_i \frac{\Psi_i(x,z)\Psi_i^*(x',z')}{k_{ti}^2} Z_{\mathrm{LSE}_i}(y,y').$$

In the above formula Φ are Ψ the LSM and LSE potentials respectively; Y_{LSM_i} and Z_{LSE_i} are the admittance and impedance, respectively, of the piecewise homogeneous transverse line representing LSM and LSE propagation in the y-direction of the i-th mode of the parallel plate waveguide formed by the side walls of the box parallel to y. These are reported in full in Appendix A.

In (1), $\tilde{\mathbf{Z}}$ is an integral operator whose kernel is given by $\mathbf{Z}$ of (2a). It is noted that the first term in (2a) gives two singular contributions, the first being the well known singularity necessary in order to expand the potentials within the source region, while the second one can be expressed as

$$\sum_i -\frac{\nabla_t\nabla_t'\Phi_i(x,z)\Phi_i^*(x',z')}{k_{ti}^2}\delta(y-y'). \tag{3}$$

This stems from just the LSM potentials and is nonvanishing on any $y = y'$ plane containing sources. Such a singularity holds no physical meaning: it is required in order to ensure continuity of the transverse electric fields that would otherwise be lost by the presence of a spurious δ-function arising from the double differentiation of Y_{LSM}. In fact, the following identity holds for the second term in (2a)

$$\begin{aligned} &(\nabla\times\nabla\times\hat{\mathbf{y}})(\nabla'\times\nabla'\times\hat{\mathbf{y}})S_{\mathrm{LSM}}(\mathbf{r},\mathbf{r}') \\ &= \left(\nabla_t\frac{\partial}{\partial y} - \hat{\mathbf{y}}\nabla_t^2\right)\left(\nabla_t'\frac{\partial}{\partial y'} - \hat{\mathbf{y}}\nabla_t'^2\right)\frac{1}{j\omega\varepsilon(y')} \\ &\quad\times\sum_i \frac{\Phi_i(x,z)\Phi_i^*(x',z')}{k_{ti}^2} Y_{\mathrm{LSM}_i}(y,y'). \end{aligned} \tag{4}$$

The electric field obtained from (1) satisfies all boundary conditions pertaining to the multilayer dielectric substrate and to the box, while the sources can be seen as volume currents induced by the fields within the strip conductors. Hence, the presence of the strip conductor s_i requires the additional condition that Ohm's law be satisfied in it, that is

$$\mathbf{E}(\mathbf{r}) = \rho\mathbf{J}(\mathbf{r}) \quad \forall\,\mathbf{r}\in\{s_i\}. \tag{5}$$

Care must be used if (5) is considered in a region whose losses are already contained in the DGF (i.e., a lossy dielectric): in this case the ohmic currents are partially included in (4) and must be subtracted from (5). This can be accomplished defining $\rho = 1/(\sigma_m - \sigma_d)$ where σ_m is the metal conductivity and σ_d the dielectric conductivity.

The system constituted by (1) and (5), yields the following integral eigenvalue equation

$$[\tilde{\mathbf{Z}} + \rho\tilde{\mathbf{I}}]\cdot\mathbf{J}(\mathbf{r}) = \mathbf{0} \quad \forall\,\mathbf{r}\in\{s_i\} \tag{6}$$

where $\tilde{\mathbf{I}}$ is the identity dyadic operator.

The latter can be solved by the Galerkin's method, by expanding the unknown current as follows:

$$J^{x,y,z}(x,y) = \sum_{s=1}^{N}\sum_{i=0}^{Nx-1}\sum_{j=0}^{Ny-1} X_{ijs}^{x,y,z}\frac{\mathrm{rect}_{ijs}(x,y)}{N_s} \tag{6a}$$

where

$$\mathrm{rect}_{ijs}(x,y) = \begin{cases} 1 & \begin{cases} \frac{w(s)}{Nx}i + p_x(s) \le x \le \frac{w(s)}{Nx}(i+1) + p_x(s) \\ \frac{t(s)}{Ny}j + p_y(s) \le y \le \frac{t(s)}{Ny}(j+1) + p_y(s) \end{cases} \\ 0 & \text{elsewhere} \end{cases} \tag{6b}$$

$w(s), t(s)$ are width and thickness respectively of the s-th strip; $p_x(s)$ and $p_y(s)$ are the x- and y-locations respectively of the strip with respect to the origin; N, N_x and N_y are the numbers of strips, those of the rectangular sub-domains in x and y, respectively, in which we have subdivided the strips. Finally N_s is the normalization constant

$$N_s = \sqrt{\frac{w(s)t(s)}{N_xN_y}}.$$

A longitudinal dependence of the type $e^{-\gamma z}$ is assumed throughout.

By an appropriate reordering of the indices, (6a) above can be written as a single sum. After substituting (6a) in (6) and by means of scalar multiplication with each basis function in turn, one recovers the following standard matrix eigenvalue equation

$$[\bar{\bar{\mathbf{Z}}} + \rho\bar{\bar{\mathbf{I}}}]\cdot\bar{\mathbf{X}} = \mathbf{0} \tag{7}$$

where $\bar{\mathbf{X}}$ is the column vector of the coefficients of the expansion (6a).

The complex propagation constants γ are then obtained by imposing the vanishing of the determinant of (7), that is, the dispersion equation

$$\det[\bar{\bar{\mathbf{Z}}} + \rho\bar{\bar{\mathbf{I}}}] = \mathbf{0}. \tag{8}$$

Solution of (8) requires employing an algorithm for the detection of complex roots such as Muller's algorithm. Once γ is found, the corresponding eigenvector is recovered from

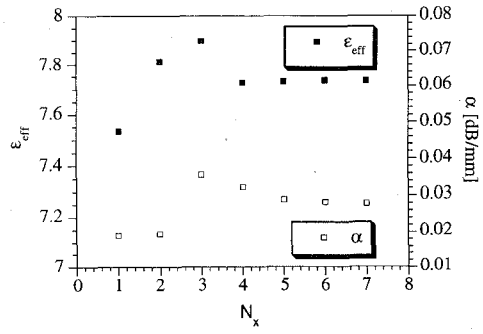

Fig. 1. Behavior of the effective dielectric constant and attenuation constant versus number of expansion functions in the x-direction (we use 5 expansion functions in the y-direction).

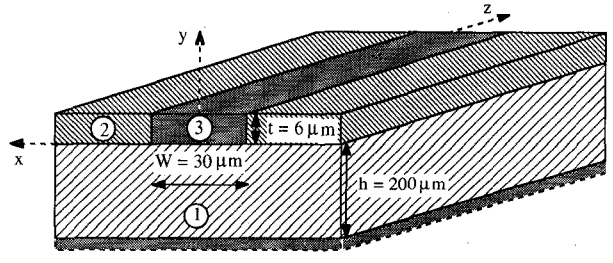

Fig. 2. Microstrip line cross-section. (1) substrate; (2) dielectric layer; (3) strip. The structure is enclosed in a large box (not shown).

(7) and the current distribution in the conductors from (6a), while (1) yields the field distribution everywhere in the box.

The variational property of (8) allows truncation of (6a) after very few terms, which suggests determining the propagation constants from a system of small dimensions and subsequently employing the roots found, in solving (7) with a larger number of expansion functions, so as to obtain a more accurate representation of the currents.

In Fig. 1 we report convergent behavior of the effective dielectric constant and the attenuation constant for increasing numbers of expanding functions in $x(N_x)$. Similar results are obtained in the y-direction where $N_y \leq N_x$.

It is noted that the choice (6a) and (6b) is not mandatory: due to the spatial formulation of the problem, it is easy to use some other basis functions in order to reduce the order of the matrix problem.

Finally we must mention the main problem related to the implementation of this method, that was the slow convergence of some series appearing in the kernel of the DGF (2). In order to overcome this drawback, we subjected it to considerable mathematical manipulation, that resulted in great improvement in computing time. This modified formulation is presented in Appendix II.

III. Results

A. Microstrip

In order to validate the proposed approach we calculate the dispersion characteristics of the structure shown in Fig. 2, comparing them in Fig. 3 with the experimental data reported in [9]: The open structure simulation was accomplished by an appropriate choice of box dimensions. It is noted how the

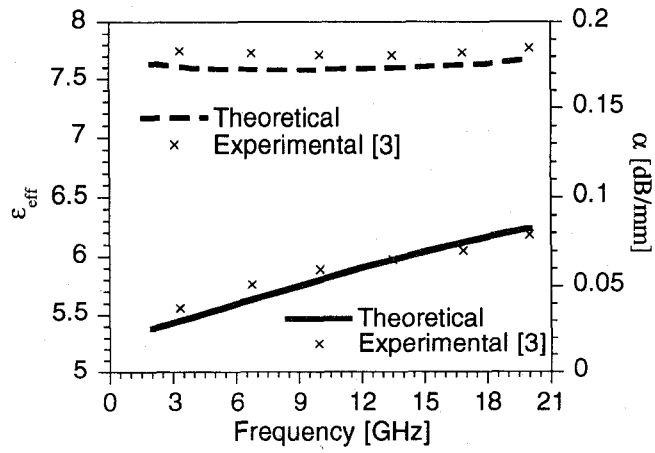

Fig. 3. Comparison between theoretical and experimental [9] values of effective dielectric constant ε_{eff} and loss α of the microstrip line shown in Fig. 2. Substrate (1): $\varepsilon_r = 12.9$, $\tan\delta = 3{\cdot}10^{-4}$; dielectric layer (2): $\varepsilon_r = 3.4$, $\tan\delta = 0.05$; strip and box conductivity (3): $\sigma = 1.77{\cdot}\ 10^7$ [Siemens/m].

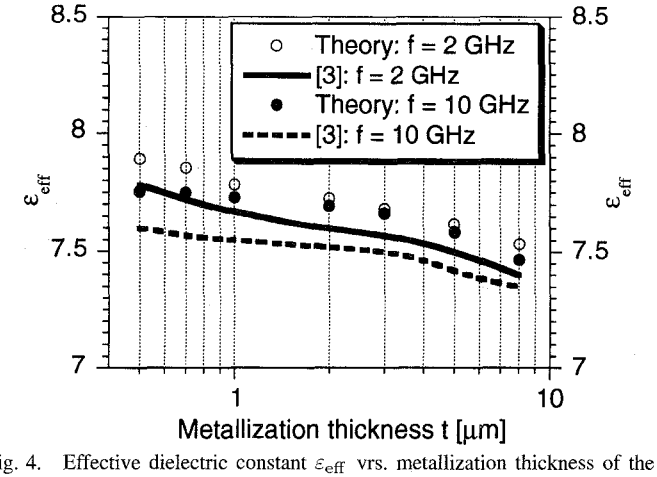

Fig. 4. Effective dielectric constant ε_{eff} vrs. metallization thickness of the microstrip line shown in Fig. 2 and comparison with numerical data reported in [3]. Substrate (1): $\varepsilon_r = 12.9$, $\tan\delta = 3{\cdot}\ 10^{-4}$; dielectric layer (2): $\varepsilon_r = 3.4$, $\tan\delta = 0.05$; strip and box conductivity (3): $\sigma = 3.333{\cdot}\ 10^7$ [Siemens/m].

present approach accurately describes the decreasing behavior of ε_{eff} over a frequency band.

The latter behavior can be attributed to the decreasing internal inductance of the conductor with increasing frequency, consistently with the fact that currents tends to redistribute toward the exterior of the conductor, an effect whose description is beyond the scope of the perturbation approach.

Next, in Figs. 4 and 5, are plotted the effective dielectric constant ε_{eff} and the attenuation α for a structure similar to that of Fig. 2 but without additional dielectric layer, for different values of the strip thickness and for two different frequencies ($f = 2$, 10 GHz): a comparison with numerical data reported in [3] shows good agreement. Note that ε_{eff} at 2 GHz is always higher than at 10 GHz; moreover, losses show a local minimum at $t = 3\delta$ as observed in [3]. The same quantities appear in Fig. 6 for two strip thicknesses (t =1.5, 3 μm) and for varying frequencies. Even in this case, it is noted that the increment of ε_{eff} appearing in the curves can not be described by means of a standard perturbation

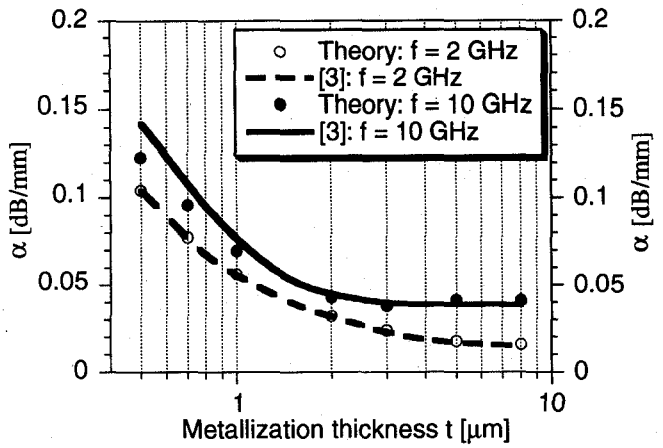

Fig. 5. Attenuation α versus metallization thickness of microstrip line shown in Fig. 2 and comparison with numerical data reported in [3]. Substrate (1): $\varepsilon_r = 12.9$, $\tan\delta = 3 \cdot 10^{-4}$; dielectric layer (2): $\varepsilon_r = 3.4$, $\tan\delta = 0.05$; strip and box conductivity (3): $\sigma = 3.333 \cdot 10^7$ [Siemens/m].

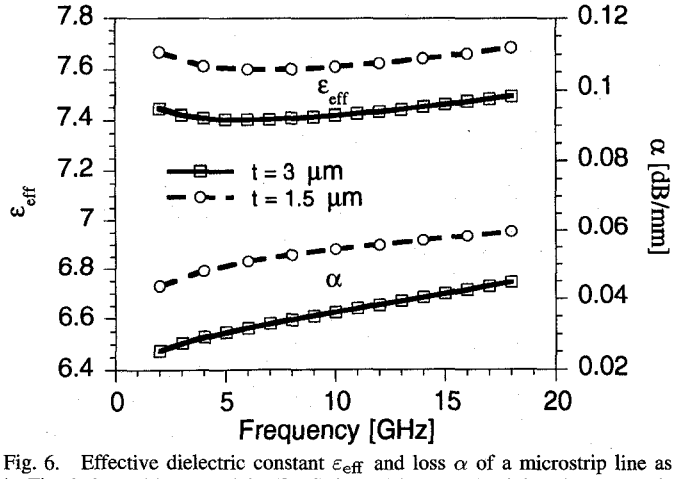

Fig. 6. Effective dielectric constant ε_{eff} and loss α of a microstrip line as in Fig. 2, but with $\varepsilon_r = 1$ in (2). Strip and box conductivity (3): $\sigma = 3.0 \cdot 10^7$ [Siemens/m].

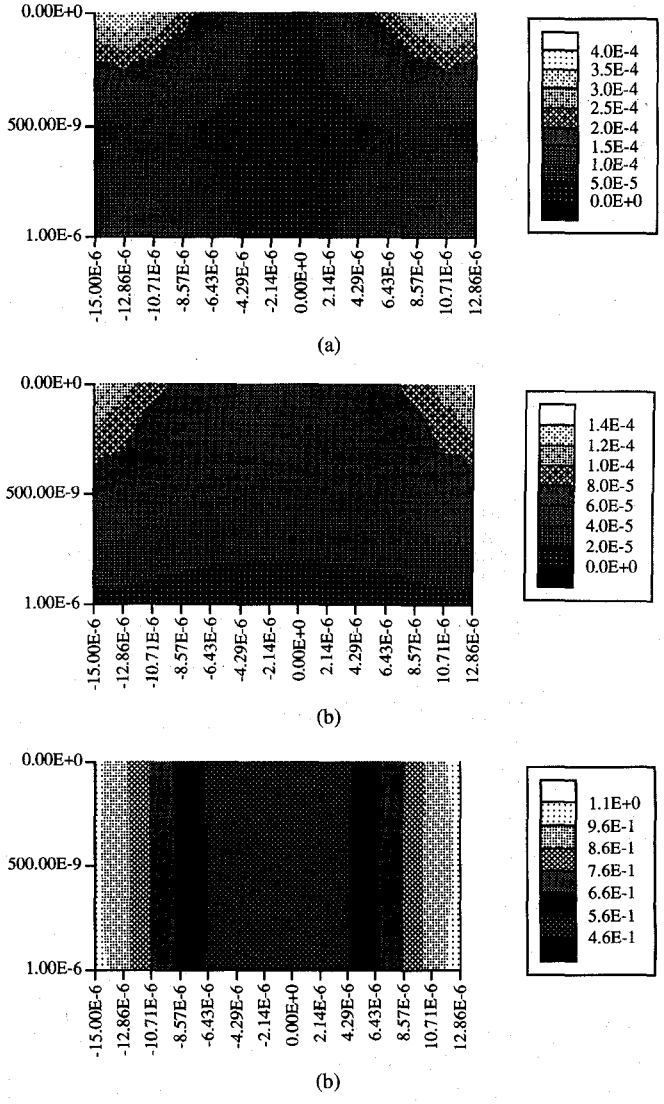

Fig. 7. (a) Magnitude of current component J_x in the strip conductor of structure simulated in Fig. 6 with $w = 30$ μm, $t = 1.5$ μm, $f = 2$ GHz. (b) Magnitude of current component J_y. (c) Magnitude of current component J_z.

approach. A modified perturbation approach, though allowing an accurate characterization of the behavior of the attenuation α, nonetheless does not permit to describe its influence on the ε_{eff}.

As already observed, the present approach provides the actual current distributions on the strip cross-section. The behavior of the three components of the current for the frequency of 10 GHz can be found in Fig. 7(a)–(c). It is seen that J_z is the main component and that all currents crowd in at the metal-dielectric interface, particularly in the neighborhood of the metal corners, even though no edge singularity is now present.

B. Unbiased FET-Structure

We report in Fig. 9(a) and 9(b) and Fig. 10(a) and 10(b) the slow wave factor and the attenuation α of the unbiased FET structures depicted, respectively, in Figs. 8(a) and 8(b). In particular, Fig. 8(b) shows the configuration proposed in [2] featuring a T-gate electrode, as required in order to limit the width of the Schottky junction at the gate, while keeping its cross-section sufficiently large; Fig. 8(a) shows the same configuration but with a standard gate instead. Consequently, the two configurations present in principle the same transconductance and our purpose is to evaluate the effect of either choice on the propagation characteristics of the unbiased configuration.

We consider a self-aligned configuration for the two highly doped regions to prevent problems of DC dissipation that the gate-drain distance (100 μm) can cause. These devices are unbiased; nevertheless we take in to account a depletion region beneath the gate electrode caused by the Schottky contact: for this region we assume a depth of about one half of the channel dimension ($d/2$).

In order to compute the channel conductivity we used the doping density proposed in [2] $N_D = 3 \cdot 10^{23}$ atoms/m^3 with a low-field mobility $\mu_n = 8500$ cm^2/V sec.

We found the three fundamental modes of the structures; each of them has a current distribution that is approximately maximum on one of the strips.

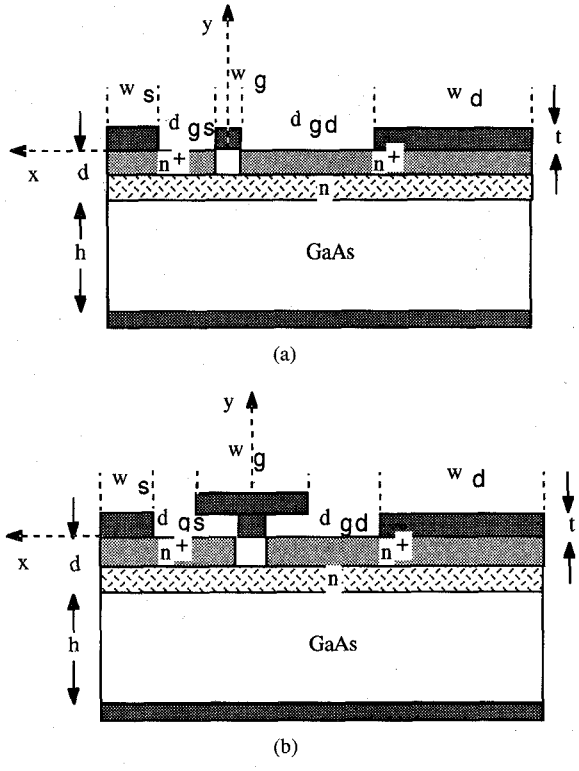

Fig. 8. Standard gate TW-FET w_s: 2 μm, w_g: 1 μm, w_d: 300 μm, d_{gs}: 10 μm, d_{gd}: 100 μm, t: 1 μm, h: 30 μm, d: 0.2 μm, substrate: $e_r = 12.9$, channel conductivity: $\sigma = 4.0 \cdot 10^4$[S/m], Strip and box conductivity: $\sigma = 3.0 \cdot 10^7$ [S/m], highly n-doped regions conductivity: $\sigma = 2.010^5$ [S/m]. The structure is enclosed in a large box, not shown. (b) Cross-section of a TWF with T-gate, for the dimensions see previous figure; in addition T-gate width: 30 μm.

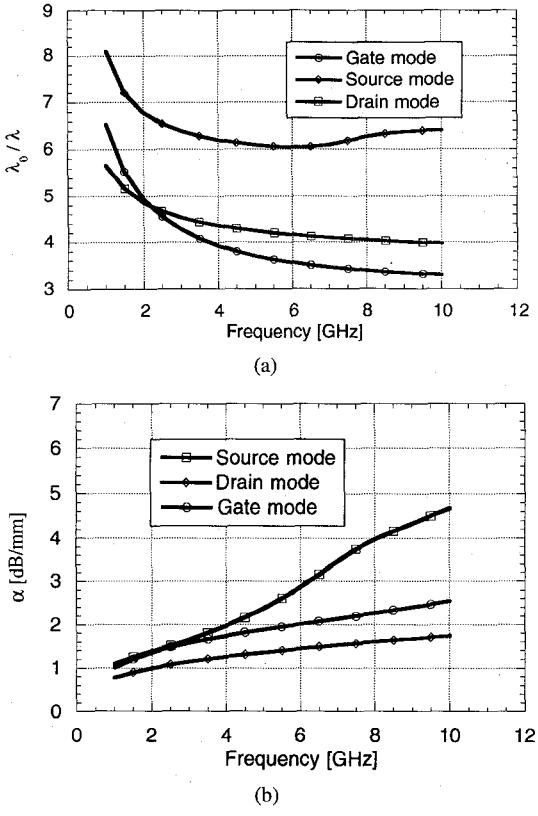

Fig. 9. (a) Slow-wave factor of the TWF shown in Fig. 8a. (b) Loss a of the TWF shown in Fig. 8(a).

In the simple gate structure all three modes show slow wave behavior explicable in terms of two different phenomena.

The gate electrode is insulated from the channel by the depletion region, giving rise to a typical MIS (Metal-Insulator-Semiconductor) configuration: in this case, the spatial dislocation of the electric and magnetic fields produces a shunt capacitance across the line representation of the gate mode.

For drain and source modes, channel and conductors losses introduce large series resistance and shunt conductance, due to the ohmic contacts with the channel region of the drain and source electrodes. All these phenomena described for the three modes increase the propagation constant thereby reducing the wave velocity. Lowering of the internal inductance of the strips due to skin effect has also same influence in the higher frequency range, as previously noted.

In the T-gate structure, instead, we observe steeply decreasing gate-mode losses, so that the behavior of λ_0/λ is the result of two different effects: on the one hand, the air gap beneath the T-bar reduces λ_0/λ, whereas on the other hand, lower conductor losses reduce the negative slope of the curve. The other two modes are quite similar in both structures.

IV. Conclusion

We report a rigorous full-wave analysis of microstrip lines for MMIC application and unbiased TW-FET structures. This is based on replacing metallizations of finite thickness, conductivity and fairly arbitrary cross-section with distributed equivalent currents and casting the dyadic Green's function of a boxed multilayer lossy substrate in a form suitable for integration over the source region. Application of Ohm's law within the metallization results in an eigenvalue equation for the currents that is solved by Galerkin's method.

This formulation is particularly suited for layered structures, as the computational load is independent of the number of dielectric layers.

Results are presented for boxed, embedded microstrip, showing very good agreement with available numerical and experimental data.

Finally, unbiased TW-FET's with standard and T-type gates are also characterized.

Appendix A

A. Scalar Dyadic Operators

We report in this section the complete expressions of the scalar dyadic operators contained in (2); these are obtained by making recourse to the result

$$Z_{\mathrm{LSM}}(y,y') = \frac{1}{\omega^2\varepsilon(y)\varepsilon(y')}\partial_y\partial_{y'}Y_{\mathrm{LSM}}(y,y') + \frac{1}{j\omega\varepsilon(y)}\delta(y-y').$$

In particular, we obtain

$$\tilde{Z}_{xx} = \sum_{n=0}^{\infty} \frac{\Psi_n(x)\Psi_n(x')}{\left(\frac{n\pi}{a}\right)^2 - \gamma^2} \times \left[\left(\frac{n\pi}{a}\right)^2 Z_{\mathrm{LSM}_n}(y,y') - \gamma^2 Z_{\mathrm{LSE}_n}(y,y')\right]$$

$$\tilde{Z}_{xy} = \sum_{n=0}^{\infty} \frac{\Psi_n(x)\Phi_n(x')}{\omega^2\varepsilon(y)\varepsilon(y')}(-1)^n\left(\frac{n\pi}{a}\right)\partial_y Y_{\mathrm{LSM}_n}(y,y')$$

$$Z_{xy}(x,y;x',y') = Z_{xy}(x',y';x,y)$$

$$\tilde{Z}_{xz} = \sum_{n=0}^{\infty} \gamma\left(\frac{n\pi}{a}\right)\frac{(-1)^n\Psi_n(x)\Phi_n(x')}{\left(\frac{n\pi}{a}\right)^2 - \gamma^2} \times [Z_{\mathrm{LSM}_n}(y,y') - Z_{\mathrm{LSE}_n}(y,y')]$$

$$Z_{zx}(x,y;x',y') = -Z_{xz}(x',y';x,y)$$

$$\tilde{Z}_{zz} = \sum_{n=0}^{\infty} \frac{\Phi_n(x)\Phi_n(x')}{\left(\frac{n\pi}{a}\right)^2 - \gamma^2} \times \left[\left(\frac{n\pi}{a}\right)^2 Z_{\mathrm{LSE}_n}(y,y') - \gamma^2 Z_{\mathrm{LSM}_n}(y,y')\right]$$

$$\tilde{Z}_{yz} = \sum_{n=0}^{\infty} \gamma\frac{\Phi_n(x)\Phi_n(x')}{\omega^2\varepsilon(y)\varepsilon(y')}\partial_{y'} Y_{\mathrm{LSM}_n}(y,y')$$

$$Z_{yz}(x,y;x',y') = -Z_{zy}(x',y';x,y)$$

$$\tilde{Z}_{yy} = \sum_{n=0}^{\infty} \frac{\Phi_n(x)\Phi_n(x')}{\omega^2\varepsilon(y)\varepsilon(y')}\left[\left(\frac{n\pi}{a}\right)^2 - \gamma^2\right] Y_{\mathrm{LSM}_n}(y,y') + \frac{1}{j\omega\varepsilon(y)}\delta(\mathbf{r}-\mathbf{r}').$$

In the above formula Y_{LSM_i} and Z_{LSE_i} are the scalar Green's admittance and impedance of the piecewise homogeneous transverse line representing LSM and LSE propagation in the y-direction of the i-th parallel plate mode: referring to the Fig. 11, a general expression for Z_n is given by

$$\mathbf{Z}_n(y,y') = \begin{cases} k_n^+ \frac{[\cos k_{y2_n} y - j z_{02_n} Y_n^+(0)\sin k_{y2_n} y]}{Y_n^+(-d)+Y_n^-(-d)} \\ [\cos k_{y1_n}(y'-d) + j z_{01_n} y_n^-(-d)\sin k_{y1_n}(y'-d)] \text{ if } y > y' \\ k_n^- \frac{[\cos k_{y1_n}(y-d)+j z_{01_n} Y_n^-(-d)\sin k_{y1_n}(y-d)]}{Y_n^+(0)+Y_n^-(0)} \\ [\cos k_{y2_n} y' - j z_{02_n} Y_n^+(0)\sin k_{y1_n} y'] \text{ if } y < y' \end{cases}$$

where k_n^+ and k_n^- are voltage ratios

$$k_n^+ \triangleq V_n(0)/V_n(-d) \text{ when the sources are in reg. 1}$$
$$k_n^- \triangleq V_n(-d)/V_n(0) \text{ when the sources are in reg. 2}$$

that can be calculated from the transmission matrix of the dielectric stack; Y_n^+ and Y_n^- are the LSM or LSE admittances respectively seen in the upper and lower direction at a given reference plane whereas z_{0in} is the characteristic impedance in the i-th region.

Expressions for Y_{LSM_i} can be obtained by duality.

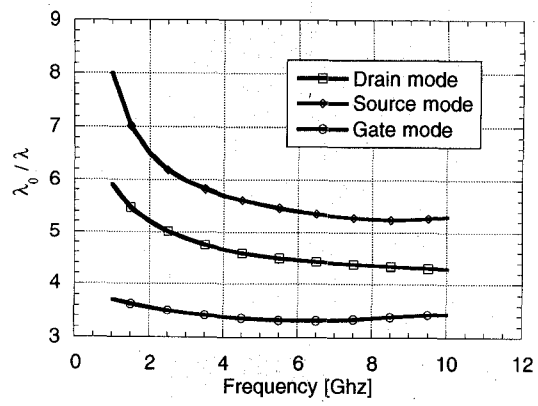

(a)

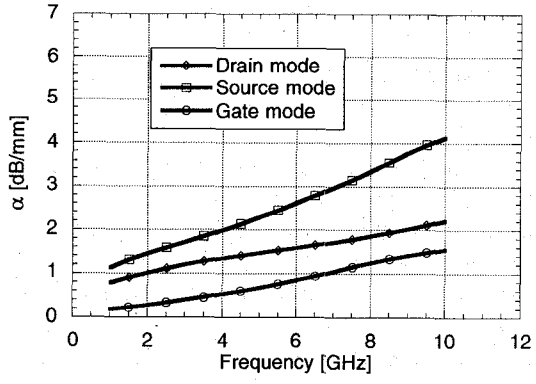

(b)

Fig. 10. (a) Slow-wave factor of the TWF shown in Fig. 8b. (b) Loss a of the TWF shown in Fig. 8(b).

APPENDIX B

A. Convergence, Modified Formulation

Some of the series appearing in the kernel of the DGF are slowly convergent. From a study of their asymptotic behavior, in fact, it appears that the most critical case arises in the expansion linking J_x and E_x to the remaining components.

Let us consider a conductor of rectangular cross section of width w and thickness t, centred at the origin and, in particular, that part of E_x that is solely due to J_x, denoted by E_{xx}. We have then

$$E_{xx}(x,y) = \int_0^t dy' \int_{-\frac{w}{2}}^{\frac{w}{2}} dx'\, Z_{xx}(x,y;x',y')J_x(x',y'). \tag{B1}$$

Upon integration by parts with respect to x', we obtain

$$E_{xx}(x,y) = \int_0^t dy'\, P(x,y;\xi,y')J_x(\xi,y')\Big|_{-\frac{w}{2}}^{\frac{w}{2}} - \int_0^t dy' \times \int_{-\frac{w}{2}}^{\frac{w}{2}} dx'\, P(x,y;x',y')\partial_{x'}J_x(x',y') \tag{B2}$$

where

$$P(x,y;x',y') = \int dx'\, Z_{xx}(x,y;x',y') \tag{B3}$$

We now observe that the first term of (B2) vanishes identically for a perfect conductor located anywhere in the cross-section,

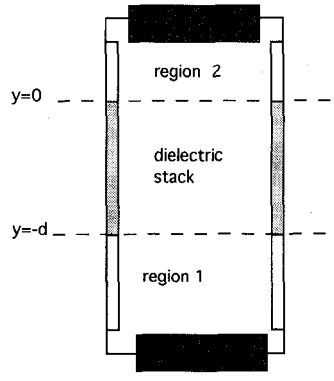

Fig. 11. Piecewise homogeneous transverse line representing LSM and LSE propagation in the y-direction of the n-th mode for the scalar Green's functions calculation.

for, the condition then holds

$$J_x\left(-\frac{w}{2}, y\right) = J_x\left(\frac{w}{2}, y\right) = 0. \tag{B4}$$

In the following, we shall assume the vanishing of the first term in (B2) to hold in any case. Various simulations, effected without employing the above hypothesis, show that a small J_x-component is generally present on the sides of the strip ($x = \pm w/2$), particularly near the lower corners, i.e. close to the substrate.

Adoption of (B4), however, does not introduce appreciable errors in the computation of either the propagation constant (a variational quantity) or of the current distribution itself, that is nonvariational.

Upon indefinite integration of E_x with respect to x, we obtain

$$\hat{\mathbf{E}}(\mathbf{r}) = -\hat{\tilde{\mathbf{Z}}} \cdot \hat{\mathbf{J}}(\mathbf{r}) \tag{B5}$$

where

$$\hat{\mathbf{E}} = \begin{bmatrix} \frac{\pi}{a}\int dx\ E_x \\ E_y \\ E_z \end{bmatrix} \qquad \hat{\mathbf{J}} = \begin{bmatrix} \frac{a}{\pi}\partial_{x'} J_x \\ J_y \\ J_z \end{bmatrix} \tag{B6}$$

and the operator $\hat{\tilde{\mathbf{Z}}}$ is the same as $\tilde{\mathbf{Z}}$ with the following substitution

$$\begin{aligned} &\hat{\tilde{Z}}_{xx} \to -\left(\frac{\pi}{a}\right)^2 \int dx \int dx'\, \tilde{Z}_{xx} \\ &\hat{\tilde{Z}}_{xy} \to \frac{\pi}{a}\int dx\, \tilde{Z}_{xy} \qquad \hat{\tilde{Z}}_{xz} \to \frac{\pi}{a}\int dx\, \tilde{Z}_{xz} \\ &\hat{\tilde{Z}}_{yx} \to -\frac{\pi}{a}\int dx'\, \tilde{Z}_{yx} \qquad \hat{\tilde{Z}}_{zx} \to -\frac{\pi}{a}\int dx'\, \tilde{Z}_{zx}. \end{aligned} \tag{B7}$$

The double integration produces a factor $(a/n\pi)^2$ in $\tilde{Z}_{xx}$ and of $(a/n\pi)$ in the remaining kernels, thereby enhancing convergence of the series.

In view of the foregoing modification, we replace in (5)

$$E_x = \rho J_x \tag{B8a}$$

by the equivalent condition

$$\int dx\ E_x(x,y) = \frac{\rho}{2}\int\int_{\text{strip}} dx'\, dy'\, |x - x'|\delta(y - y') \times \partial_{x'} J_x(x', y'). \tag{B8b}$$

The system to be solved is now constituted by (B8b) and (B5).

Some care is necessary in order that condition (B4) be satisfied by the expansion functions too; a possible expansion for J_x is in term of triangular impulses.

Note that the condition (B4) also acts as an additional constraint, reducing the number of spurious solutions.

REFERENCES

[1] W. Heinrich and H. L. Hartnagel, "Wave propagation on MESFET electrodes and its influence on transistor gain," *IEEE Trans. Microwave Theory Tech.*, vol. MTT-35, no. 1, pp. 1–8, Jan. 1987.

[2] S. D'Agostino, G. D'Inzeo, and L. Tudini, "Analytical modeling and design criteria for traveling-wave FET amplifiers," *IEEE Trans. Microwave Theory Tech.*, vol. 40, no. 2, , pp. 202–208, Feb. 1992.

[3] W. Heinrich, "Full wave analysis of conductor losses on MMIC transmission lines," *IEEE Trans. Microwave Theory Tech.*, vol. 38, no. 10, pp. 1468–1472, Oct. 1990.

[4] T. Rozzi, G. Gerini, and M. Farina, "Efficient characterization of millimetric TW FET's with finite metallization," in *Proc. 23rd Euro. Microwave Conf.*, Madrid, Spain, 1993, pp. 708–709.

[5] T. Shibata and E. Sano, "Characterization of MIS structure coplanar transmission lines for investigation of signal propagation in integrated circuits," *IEEE Trans. Microwave Theory Tech.*, vol. 38, no. 7, pp. 881–890, July 1990.

[6] K. Han and T. T. Y. Wong, "Coupled-wave small-signal transient analysis of GaAs distributed amplifier," *IEEE Trans. Microwave Theory Tech.*, vol. 38, pp. 23–29, Feb. 1990.

[7] M. B. Anan *et al.*, "A traveling-wave high electron mobility transistor," *IEEE Trans. Microwave Theory Tech.*, vol. MTT-41, no. 4, pp. 624–630, 1993.

[8] L. B. Felsen and N. Marcuvitz, *Radiation and Scattering of Waves*. Englewood Cliffs, NJ: Prentice-Hall, 1973, chs. 1, 2.

[9] H. J. Finlay *et al.*, "Accurate characterization and modeling of transmission lines for GaAs MMIC's," *IEEE Trans. Microwave Theory Tech.*, vol. 36, no. 6, pp. 961–967, June 1988.

[10] F. Alessandri *et al.*, "Propagation characteristics of lossy distributed GaAs FET structures," in *1992 IEEE MTT-S, Int. Microwave Symp. Dig.*, Albuquerque, NM, 1992, pp. 963–966.

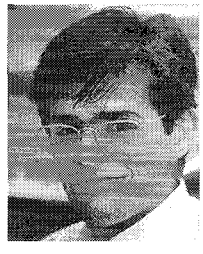

Marco Farina, was born in Luzern, Switzerland, in 1966. He completed the M. Eng. in electronics at the University of Ancona and was awarded the summa cum laude degree in I990. He is currently a final year Ph.D. candidate in the same department.

His thesis topic is the rigorous field analysis of TW-FET's and slow-wave structures. Ing. He is the author of six papers in this area.

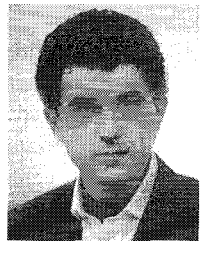

Giampiero Gerini (S'92–M'92–M'92) was born in Italy in 1962. He received the M. Eng. degree (summa cum laude) in electronic engineering in 1988 and the Ph.D. degree in electronic engineering (electromagnetic theory) in 1993, both from the University of Ancona.

Since 1989 he has been with the Department of Electronics and Automatics at the University of Ancona as a research fellow. His research is mainly devoted to the modelling of passive millimetric wave devices and antennas. He is now with the European Space Agency (ESA-ESTEC, Noordwijk, The Netherlands).

Tullio Rozzi (M'66–SM–74–F'90) obtained the degree of 'Dottore' in physics from the University of Pisa in 1965 and the Ph. D. degree in electronic engineering from Leeds University in 1968. In June 1987 he received the D. Sc. degree from the University of Bath, Bath, U.K.

From 1968 to 1978 he was a research scientist at the Philips Research Laboratories, Eindhoven, the Netherlands, having spent one year (1975) at the Antenna Laboratory, University of Illinois, Urbana. In 1978 he was appointed to the Chair of Electrical Engineering at the University of Liverpool and was subsequently appointed to the Chair of Electronics and Head of the Electronics Group at the University of Bath in 1981, where he also held the responsibility of Head of the School of Electrical Engineering on an alternate three-year basis. Since 1988 He has been professor of antennas in the Department of Electronics and Control, University of Ancona, Italy, while remaining a visiting professor at Bath University.

Dr. Rozzi was awarded the Microwave Prize by the IEEE Microwave Theory and Technique Society in 1975. He is also a Fellow of the IEE (UK).